The density of ambient black carbon retrieved by a new method: implications to CCN prediction

Jingye Ren[1, 2], Fang Zhang[2*], Lu Chen[1], Jieyao Liu[1]

[1]*College of Global Change and Earth System Science, Beijing Normal University, Beijing 100875, China*

[2]*Shenzhen Key Laboratory of Organic Pollution Prevention and Control, School of Civil and Environmental Engineering, Harbin Institute of Technology (Shenzhen), 518055 Shenzhen, China*

***Correspondence to:* Fang Zhang (zhangfang2021@hit.edu.cn)**

Abstract.

The effective density of black carbon (BC) is a crucial factor relevant to its aging degree that would add uncertainty in evaluating its climate effect. Here, we have developed a new method to retrieve the effective density of internally mixed BC in the atmosphere combining field observations conducted during 15 November -14 December 2016 in urban Beijing with the Köhler theory. The uncertainty of the retrieval method was evaluated within ±30 %, which is primarily caused by assumptions of the hygroscopic parameter of organics and the fraction of primary organic aerosols in non-hygroscopic or hygroscopic mode. Using the method, we obtain that the ambient internally mixed BC, accounting for 80±20 % of total BC aerosol particles, is retrieved with a campaign mean density of 1.1±0.6 g cm^{-3} during the observed periods. The retrieved result is comparable with that reported in the Literature. By applying a lower (0.14 g cm^{-3}) and upper (2.1 g cm^{-3}) limit of the retrieved BC density in cloud condensation nuclei (CCN) number concentrations (N_{CCN}) estimation, we derived that neglect of such variations in BC density would lead to an uncertainty of -28 %~11 % in predicting N_{CCN} at supersaturations of 0.23 % and 0.40 %. We also find that the N_{CCN} is more sensitive to the variations of BC density when it is <1.0 g cm^{-3}. This illustrates a necessity of accounting for the effect of BC density on CCN activity closer to source regions where the BC particles are mostly freshly emitted. The CCN closure achieves when introducing the retrieved real-time BC density and mixing state. This study provides a unique way of utilizing field measurements to infer ambient BC density and

删除了: on

删除了: -

删除了: literatures

删除了: led

highlights the importance of applying variable BC density values in models when predicting CCN and assessing its relevant climate effect.

1 Introduction

Black carbon (BC) aerosols, as the major absorber of solar radiation, play a vital role in energy budget and climate of the earth-atmosphere system by affecting the radiative forcing and cloud properties (Flanner et al., 2007; Ramanathan and Carmichael, 2008). The light-absorbing capability induced by BC is related to its density and morphology (Zhang et al., 2008; Rissler et al., 2014), which can be modified after mixing with other atmospheric aerosol particles (Khalizov et al., 2009; Xue et al., 2009). Changes in its physicochemical properties would also regulate its ability to serve as cloud condensation nuclei (CCN) and further indirectly affect the radiative balance by affecting the clouds process (Yuan et al., 2008; Wang et al., 2011). Owing to the complex evolution of the mixing state, density and morphology of BC, the contribution of BC particles to CCN budgets is still not well understood.

BC particles, with diesel vehicles, industrial and residential coal combustion as major sources, are ubiquitous in urban environments (Bond et al., 2013; Dameto et al., 2017; Li et al., 2017; Liu et al., 2019a). The mixing state of BC describes the distribution of the bare BC and coating masteries among the aerosol population. Typically, freshly generated BC exists in the form of chain aggregates and initially uncoated, which is known as externally mixed BC (Ex-BC). When the BC particles were emitted, they generally mix with other materials by condensation, coagulation,

and other processes (Riemer et al., 2004; Zhang et al., 2008; Liu et al., 2013; Zhang et al., 2020a), forming the internally mixed BC (In-BC) particles consisting of BC core and other chemical components (Cheng et al., 2006; Zhang et al., 2016). The BC structure would be more compact with regular shapes (Pagels et al., 2009; Zhang et al., 2008; Wang et al., 2017), and the effective density of internally mixed BC are changed accordingly with the reconstruction (Liu et al., 2019b). The density and morphology of BC particles are closely related to its sources, mobility size, coating thickness, coating material and its chemical composition (Zhang et al., 2008; Pagels et al., 2009; Peng et al., 2016; Zhang et al., 2022). A wide range of BC density has been reported in previous studies (Lide 1992; McMurry et al., 2002; Park et al., 2004; Kiselev et al., 2010). Recent field measurements have indicated that the average BC density is ~1.2 g cm^{-3} in the ambient atmosphere (Zhang et al., 2016). Field measurements have also indicated that a considerable fraction of externally mixed/uncoated BC exists (Clarke et al., 2004; Cheng et al., 2012), although a higher proportion of internally mixed/aged BC particles in the ambient atmosphere were observed (Schwarz et al., 2008; Massoli et al., 2015; Chen et al., 2020). In climate models, the BC was generally assumed completely internally mixed and treated to have a void-free spherical structure and a density value of 1.8 g cm^{-3} (Bond et al., 2013). This may lead to bias in estimating the climate effect driven by BC.

删除了: Mcmurry

删除了: -

Previous study based on a case study show that when the aging degree of ambient particles is low, the BC density (~1.8 g cm^{-3}) under the spherical assumption will lead to the overestimation of particle hygroscopicity by 40-50 % and the overestimation can

be explained almost 100 % using the effective density of fresh BC (~0.45 g cm^{-3}) (Fan et al. 2020). This indicates the importance of using reasonable BC density values in the calculation of particle hygroscopicity. In addition, when estimating the CCN number concentration, a significant bias of –35 % ~ +20 % was found due to the assumption of particle mixing state (Ren et al., 2018). However, these studies have not yet accounted for such impact of BC density and mixing state on CCN prediction due to lack of real time measurement data.

The mixing state and the density of BC particles are usually directly measured by several techniques, such as an integrated system of a volatility tandem differential mobility analyzer and a single particle soot photometer (VTDMA-SP2) (Zhang et al., 2016), or a differential mobility analyzer with a SP2 (DMA-SP2) (Olfert et al., 2007; Rissler et al., 2014; Wu et al., 2019), and a differential mobility analyzer–centrifugal particle analyzer–single-particle soot photometer (DMA–CPMA–SP2) system (Liu et al., 2019b; Yu et al., 2020), etc. However, such techniques or measurements are not available in many previously conducted filed campaigns. In this study, we develop a novel method for retrieving the mixing state and effective density of ambient BC particles by combining field measured hygroscopic growth factor and aerosol chemical composition and Köhler theory (Petters and Kreidenweis, 2007). The uncertainty of the new retrieval method was evaluated. The retrieved results were also compared and validated with existing observations. In addition, the effect of BC density and mixing state on prediction of CCN number concentrations is further evaluated through a sensitivity and closure test by accounting for the retrieved real-time variations of BC

density and mixing state.

2 Field measurements and methodology

2.1 Field measurements

Measurements in this study were conducted from 15 November to 14 December 2016 at a typical urban site of Beijing (39.97°N, 116.37°E, 49 m above sea level). The site locates at the Institute of Atmospheric Physics, Chinese Academy of Sciences, which is mainly influenced by the surrounding cooking, road traffic and residential coal burning emissions during the home heating periods (Sun et al., 2016). The detailed information about the sampling site was presented in previous studies (Sun et al., 2015; Zhang et al., 2019). The number concentration of condensation nuclei (CN) at each size was measured by a scanning mobility particle sizer, which is equipped with a differential mobility analyzer (DMA; model 3081, TSI) and a condensation particle counter (CPC; model 3772, TSI). Subsequently, the mono-dispersed particles were introduced into a Droplet Measurement Technologies CCN counter (CCNc, DMT; Lance et al., 2006) to measure CCN number concentration. A hygroscopic tandem differential mobility analyzer (HTDMA) system was used to measure the hygroscopic growth factor (Gf) (Tan er al., 2013). Here, four diameters of 40, 80, 110, 150, and 200 nm are selected in the campaign. Gf is defined as the ratio of the mobility diameter at the given RH to the dry diameter (Petters and Kreidenweis, 2007). The nonrefractory submicron aerosol chemical composition was measured by an Aerodyne high-resolution time-of-flight aerosol mass spectrometer (HR-AMS; Xu et al., 2019),

including sulfate, nitrate, ammonium, chloride, and organics. Two factors, including a non-hygroscopic primary organic aerosol (POA) and hygroscopic secondary organic aerosol (SOA) were classified by positive matrix factorization (PMF) with PMF algorithm (v4.2) method (Paatero and Tapper, 1994) and followed the procedures reported in Ulbrich et al. (2009). The refractory black carbon mass loading was measured by an aethalometer (model AE33, Magee Scientific Corporation). Both the nonrefractory materials and BC mass concentration were measured with diameters < 1.0 μm. The detailed description of the instrument operation and data process have been described in details elsewhere (Ren et al., 2018; Xu et al., 2019; Zhang et al., 2019; Fan et al., 2020).

2.2 Retrieving the mixing state and density of BC

2.2.1 Retrieving the mixing state of BC

The Gf probability distribution function (Gf-PDF) for a specified diameter can be retrieved firstly based on the TDMAinv algorithm (Gysel et al., 2009). The κ-PDF can be further calculated based on the Gf-PDF (Fan et al., 2020). Size-resolved κ is derived using κ-Köhler theory based on hygroscopic growth factor (Gf) (Petters and Kreidenweis, 2007),

$$\kappa_{gf} = (\mathrm{Gf}^3 - 1) \cdot \left[\frac{1}{\mathrm{RH}} \exp\left(\frac{4\sigma_{s/a} M_w}{RT\rho_w \mathrm{D_d Gf}}\right) - 1\right] \quad (1)$$

where Gf is hygroscopic growth factor, RH is the relative humidity in the HTDMA (90 %), D_d is the dry diameter, $\sigma_{s/a}$ is assumed to be the surface tension of pure water,

158 R is the universal gas constant, T is the temperature, M_w and ρ_w is the molecular mass,
159 and the density of water, respectively.
160 The κ-PDF patterns of particles in different sizes always present two modes: nearly
161 hydrophobic (NH) mode with $\kappa_{gf} \leqslant 0.1$ and more hygroscopic (MH) mode with $\kappa_{gf} >$
162 0.1 (Fig. S1). Firstly, based on the κ-PDF patterns, the number fraction (NF) of the total
163 nearly hydrophobic group with the boundary of [0, 0.1] was calculated according to the
164 following equation:
165 $$NF = \int_0^{0.1} c(\kappa, D_p)\, d\kappa \quad (2)$$
166 here, the κ-PDF, represented by c (κ, D_p), was normalized as $\int c(\kappa, D_p)\, d\kappa = 1$, where
167 κ can be replaced by κ_{gf}, D_p is the selected electrical mobility diameter in the campaign.
168 The nearly hydrophobic mode consists of both externally mixed POA (Ex-POA or
169 bare POA) and externally mixed BC (Ex-BC). Since the number fraction of the nearly-
170 hydrophobic POA would change with the emission and aging processes, in this study,
171 we have applied different values for the number fractions of hydrophobic POA (NH-
172 POA) under clean (91 %), moderately polluted (70 %), and heavily polluted conditions
173 (31 %) by referring the literature (Liu et al., 2021a), as shown in Fig. S2. The number
174 concentration of Ex-BC was then calculated using the total number fraction of NH
175 mode minus the number of NH-POA.
176 $$N_{POA-containing} = N_{total} \times NF_{POA-containing}$$
177 $$N_{bare-POA} = N_{POA-containing} \times NF_{bare-POA}$$
178 $$N_{Ex-BC} = N_{NH} - N_{bare-POA} \quad (3)$$
179 where $N_{POA\text{-}containing}$ and $NF_{POA\text{-}containing}$ are the number concentration and fraction of

POA-containing particles, N_{total} is the total number concentration, $N_{bare\text{-}POA}$ and $NF_{bare\text{-}POA}$ are the number concentration and fraction of bare POA particles, and N_{NH} is the number of nearly hydrophobic group.

The number size distribution of the externally mixed BC ($n_{Ex\text{-}BC}$ (log D_p)) can be calculated based on the particle number size distribution (PNSD) and the number fraction of the hydrophobic mode of BC ($NF_{Ex\text{-}BC}$) as follows:

$$n_{Ex-BC}(\log Dp) = NF_{Ex-BC} \times n\ (\log Dp) \quad (4)$$

where n (log D_p) is the function of the aerosol number size distribution, D_p is the mobility diameter.

By assuming that the particles are spherical (Rader and McMurry, 1986), the mass size distribution of Ex-BC ($M_{Ex\text{-}BC}$) was obtained as follows:

$$M_{Ex-BC}(\log Dp) = \frac{\pi}{6} {D_p}^3 \rho n_{Ex-BC}(\log Dp) \quad (5)$$

where D_p is the mobility diameter, ρ is the effective density of Ex-BC, and $n_{Ex\text{-}BC}$ (log D_p) is the function of the number size distribution of Ex-BC, respectively. By reviewing and summarizing the existing results, we show that typical values of density for the freshly emitted or externally mixed BC observed in the winter of urban Beijing or North China Plain span over 0.14-0.50 g cm^{-3}, with mean of ~0.40±0.10 g cm^{-3} (Fig. S3), in the size range of 100 to 300 nm, where the mass concentration of externally mixed BC mostly concentrated (Geller et al., 2006; Peng et al., 2016, 2017; Wu et al., 2019; Liu et al., 2020; Zhao et al., 2022). Therefore, an average $\rho_{Ex\text{-}BC}$ of 0.4 g cm^{-3} was used for calculating the mass concentration of externally mixed BC in our study. Uncertainty analyses due to the variations of $\rho_{Ex\text{-}BC}$ were given in section 2.3.

删除了: -

删除了: about

删除了: spans

删除了: accounted for a large proportion in urban Beijing

删除了: -mixed BC in our study. The uncertainty analysis exhibits that the variations of the $\rho_{Ex\text{-}BC}$ could lead to an average deviation of ±10 % in the calculating In-BC density (Fig. 3e) by increasing the $\rho_{Ex\text{-}BC}$ from 0.1 to 0.6 g cm^{-3}, showing a small impact on the retrieved result.

The mass size distribution of Ex-BC was fit using the log-normal distribution as shown in Fig. S4 (Wu et al., 2017; Liu et al., 2019a; Zhao et al., 2022). Thus, the bulk mass concentration of Ex-BC can be calculated from the integration of the mass size distribution:

$$m_{\mathrm{Ex-BC}} = \int_{D_{start}}^{D_{end}} M_{\mathrm{Ex-BC}}(\log\ D_p)\ d\ \log(D_p) \quad (6)$$

$$m_{\mathrm{In-BC}} = m_{\mathrm{BC}} - m_{\mathrm{Ex-BC}} \quad (7)$$

where D_{start} and D_{end} are the lower and upper size limit, $M_{\mathrm{Ex\text{-}BC}}$ (log D_p) is the function of the Ex-BC mass size distribution. We then obtained the bulk mass concentration of internally mixed BC ($m_{\mathrm{In\text{-}BC}}$) by subtracting $m_{\mathrm{Ex\text{-}BC}}$ from the bulk BC mass concentration measured by AE33 in equation 7. It should be noted that the mass concentration of BC obtained from AE33 based on aerosol light absorption may lead some uncertainty, as has been further addressed in Section 2.3.

2.2.2 Retrieving the density of BC

For retrieval of the density of BC, the principal idea is to use the measured κ_{gf} to calculate the density of BC based on the Zdanovskii–Stokes–Robinson (ZSR) mixing rule (Stokes and Robinson, 1966; Zdanovskii, 1948) with the chemical composition measured by AMS (Petters & Kreidenweis, 2007). In the retrieval, several aspects are concerned. First, since the ZSR rule assumes the aerosol particles are internally mixed, the κ_{gf} value of the more MH mode ($\kappa_{gf\text{-}MH}$) is thus applied for retrieving the density of internally mixed BC. Second, since the size distribution of BC number concentration is usually with peaks between 100 and 200 nm (Liu et al., 2019a; Yu et al., 2020; Zhao et

删除了: is to assume

al., 2022), the $\kappa_{gf\text{-}MH}$ value of particles in accumulation mode was averaged and applied for the retrieval. Previous studies showed an independence of $\kappa_{gf\text{-}MH}$ on particle size when the D_p >100 nm during the campaign period (Fan et al., 2020). Therefore, the average of $\kappa_{gf\text{-}MH}$ in accumulation mode is reasonable for the determination of the In-BC density. In addition, because the inversion including measurements from HTDMA and HR-AMS, a total mass closure of the measured aerosol particles was conducted between the two techniques by comparing the mass concentration of PM_1 and the results are well consistent (Fig. S6). The density of internally mixed BC (In-BC), $\rho_{In\text{-}BC}$ is then derived from the following equations:

$$\kappa_{gf-MH} = \kappa_{chem} = \sum_i \varepsilon_i \kappa_i = \frac{v_{inorg}}{v_{total}}\kappa_{inorg} + \frac{v_{SOA}}{v_{total}}\kappa_{SOA} + \frac{v_{In-POA}}{v_{total}}\kappa_{POA} + \frac{v_{In-BC}}{v_{total}}\kappa_{BC} \quad (8)$$

where $\kappa_{gf\text{-}MH}$ is the hygroscopic parameter of the more hygroscopic (MH) mode, κ_{chem} is the hygroscopic parameter of aerosol particles in the mixed composition and can be calculated based on chemical volume fractions using a simple rule (Stokes and Robinson, 1966; Petters & Kreidenweis, 2007), κ_i is the hygroscopic parameter of each pure composition and ε_i is the volume faction of the individual components in the internally mixed particle. v_{inorg}, v_{SOA} and $v_{In\text{-}POA}$ are the volume of the inorganic, SOA and internally mixed POA species, and can be calculated as follows: $v_{inorg} = \frac{m_{inorg}}{\rho_{inorg}}$, $v_{SOA} = \frac{m_{SOA}}{\rho_{SOA}}$, and $v_{In-POA} = \frac{m_{In-POA}}{\rho_{POA}}$. v_{total} is the total volume of all the species and can be written as $v_{total} = \frac{m_{inorg}}{\rho_{inorg}} + \frac{m_{SOA}}{\rho_{SOA}} + \frac{m_{In-POA}}{\rho_{POA}} + \frac{m_{In-BC}}{\rho_{In-BC}}$. In equation (8), κ_{BC} and κ_{POA} are assumed to be 0. So, the total volume v_{total} can be further written as $v_{total} = \frac{v_{inorg}\kappa_{inorg} + v_{SOA}\kappa_{SOA}}{\kappa_{gf-MH}}$. The volume of internally mixed $v_{In\text{-}BC}$ can be calculated as follows,

$$v_{In-BC} = \frac{v_{inorg}\kappa_{inorg} + v_{SOA}\kappa_{SOA}}{\kappa_{gf-MH}} - v_{inorg} - v_{SOA} - v_{In-POA}$$

删除了: S5

删除了: internal-

移动了(插入) [1]

移动了(插入) [2]

移动了(插入) [3]

$$= \frac{\frac{m_{inorg}}{\rho_{inorg}}\kappa_{inorg} + \frac{m_{SOA}}{\rho_{SOA}}\kappa_{SOA}}{\kappa_{gf-MH}} - \frac{m_{inorg}}{\rho_{inorg}} - \frac{m_{SOA}}{\rho_{SOA}} - \frac{m_{In-POA}}{\rho_{POA}} \quad (9)$$

Then, the $\rho_{\text{In-BC}}$ can be calculated based on its mass concentration and volume as follows:

$$\rho_{In-BC} = \frac{m_{In-BC}}{\left(\frac{\frac{m_{inorg}}{\rho_{inorg}}\kappa_{inorg} + \frac{m_{SOA}}{\rho_{SOA}}\kappa_{SOA}}{\kappa_{gf-MH}} - \frac{m_{inorg}}{\rho_{inorg}} - \frac{m_{SOA}}{\rho_{SOA}} - \frac{m_{In-POA}}{\rho_{POA}}\right)} \quad (10)$$

where, $m_{\text{In-BC}}$ is the mass concentration of internally mixed BC, m_{inorg} and m_{SOA} are the mass concentrations of the inorganic species and SOA, which are measured by the AMS. $m_{\text{In-POA}}$ is the mass concentrations of internally mixed POA and can be calculated through subtracting the mass fraction of NH-POA from the total mass concentrations of POA. ρ_{inorg}, ρ_{SOA} and ρ_{POA} are the density of the inorganic species, SOA and POA. Since the AMS measures the concentrations of the organic and inorganic ions, including SO_4^{2-}, NO_3^-, NH_4^+, Cl^-. Here inorganic species were derived by applying a simplified ion pairing scheme (Gysel et al., 2007) to convert mass concentrations of ions to the inorganic salts as follows:

$$n_{NH_4NO_3} = n_{NO_3^-}$$

$$n_{NH_4HSO_4} = \min(2n_{SO_4^{2-}} - n_{NH_4^+} + n_{NO_3^-}, n_{NH_4^+} - n_{NO_3^-})$$

$$n_{(NH_4)_2SO_4} = \max(n_{NH_4^+} - n_{NO_3^-} - n_{SO_4^{2-}}, 0)$$

$$n_{H_2SO_4} = \max(0, n_{SO_4^{2-}} - n_{NH_4^+} + n_{NO_3^-}) \quad (11)$$

where n represents the number of moles, and the mass concentrations were obtained by the number of moles times the molar mass of each inorganic salts. Because the value of the $n_{H_2SO_4}$ was zero in this campaign. Three inorganic salts including NH_4HSO_4, $(NH_4)_2SO_4$, and NH_4NO_3 were applied in our study. The densities for inorganic salts were taken from previous studies (Gysel et al., 2007; Wu et al., 2016). Here the densities for three inorganics are 1.78, 1.77 and 1.72 g cm^{-3}, respectively. By summarizing the

删除了: 9

删除了: 10

删除了: then

删除了: maximum

previous studies (Gysel et al., 2007; Dinar et al., 2006), 1.4 g cm^{-3} was selected as the density of SOA (ρ_{SOA}). The density of POA (ρ_{POA}) is assumed to be 1.0 g cm^{-3} for urban environments, which is similar to the that of the lubricating oil (Wu et al., 2016). Since the cooking organic aerosols represent a high contribution to POA in urban environments, we choose the mean density of the rapeseed oil and oleic acid (~0.85 g cm^{-3}) (Reyes-Villegas et al., 2018) to evaluated the result as shown in section 2.3. The values of κ for inorganic components are 0.56 for NH_4HSO_4, 0.48 for $(NH_4)_2SO_4$ and 0.58 for NH_4NO_3, along with the best-fit values for the three inorganic salts (Petters & Kreidenweis, 2007 and Gunthe et al., 2009). The κ_{SOA} is assumed to be 0.15 according to the field studies in urban areas (Chang et al., 2010; Kawana et al., 2016).

Note that the method fails to retrieve the BC density when organic accounts for a large fraction (>60 %). This is because that a higher fraction of OA usually corresponds to lower total volume of all the species (Fig. S7), yielding negative values for $v_{In\text{-}BC}$ introduced in equation 9. As a result, 61 % of the data observed during the campaign were valid for calculating the BC density.

$v_{In-BC} = \frac{v_{inorg}\kappa_{inorg}+v_{SOA}\kappa_{SOA}}{\kappa_{gf-MH}} - v_{In-POA}$Similarly, the bulk density of BC ($\rho_{bulk\text{-}BC}$) is calculated with the same method as that for calculating the $\rho_{In\text{-}BC}$. When calculating the $\rho_{bulk\text{-}BC}$, the bulk κ_{gf} value measured by HTDMA is applied assuming that all the aerosol particles are internally mixed.

2.3 Uncertainties and limitations

For the retrieval, the assumptions on the values of κ_{SOA}, ρ_{POA}, ρ_{SOA} and $\rho_{Ex\text{-}BC}$ as

删除了: Considering

删除了: a density of 0.85 g cm^{-3} chosen as

删除了: for

删除了: was also used

删除了: , this

删除了: organics account

删除了: S6

删除了: 11

上移了 [2]: v_{In-BC}

上移了 [1]: $= \frac{v_{inorg}\kappa_{inorg}+v_{SOA}\kappa_{SOA}}{\kappa_{gf-MH}}$

上移了 [3]: $-v_{In-POA}$

删除了:

删除了: $-v_{inorg} - v_{SOA}$

删除了: (11)

删除了: with the assumption of

well as the fraction of primary organic aerosols in non-hygroscopic or hygroscopic mode would add uncertainty in the inferred values of ambient internally mixed BC density. For example, the freshly emitted POA particles might consistently be coated with the secondary particles during the aging process, resulting in changes of the $NF_{NH\text{-}POA}$. However, a real-time variation of the $NF_{NH\text{-}POA}$ is not yet available due to the lack of such measurements data. Applying only the rough fractions of hydrophobic POA for

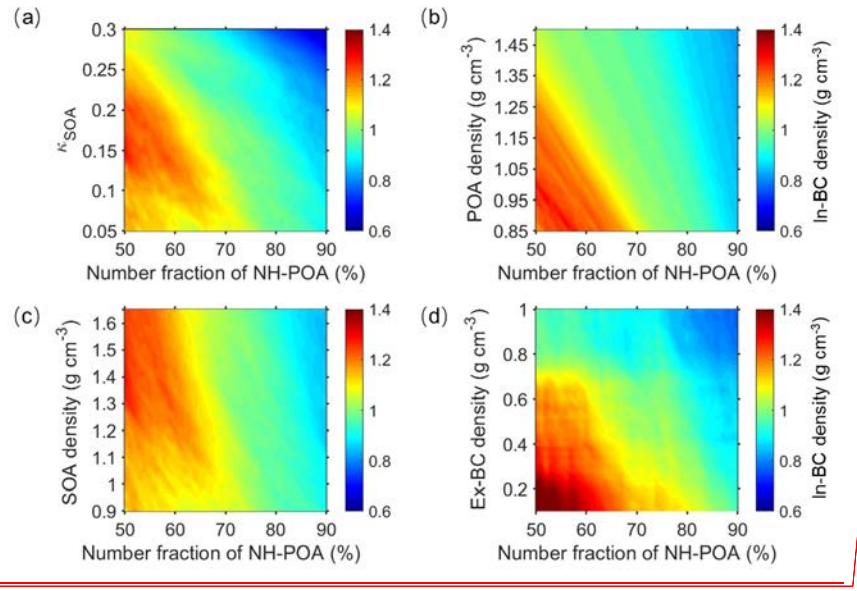

Figure 1. Sensitivities of In-BC density to the variations in the number fraction of nearly hydrophobic (NH) POA and hygroscopic parameter of OA (k_{SOA}) (a), POA density (b), SOA density (c) and the externally mixed BC density (d).

three different atmospheric conditions could still cause uncertainties. Also, the densities of POA and SOA may differ due to their precursors, emission sources and the formation mechanisms in ambient atmosphere (Alfarra et al., 2006; Reyes-Villegas et al., 2018). And the density of Ex-BC is generally characterized by the morphology and size (Wu

删除了:

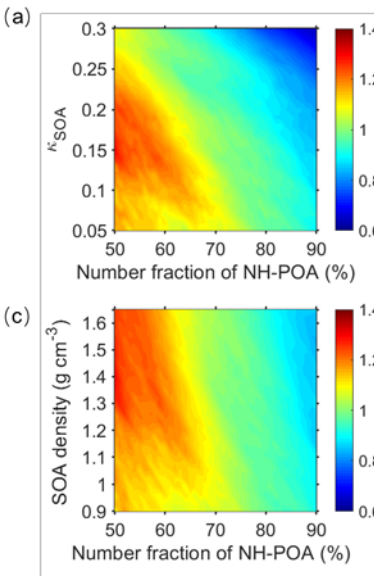

移动了(插入) [4]

删除了: only under

et al., 2019). In addition, the value of κ_{SOA} spans largely due to the variability in the emissions of gas precursors and formation processes under different atmospheric conditions (Zhang et al., 2015; Liu et al., 2021b). Therefore, we examined the sensitivities of In-BC density to the variations of these factors, as exhibited in Fig. 1 and Fig.2.

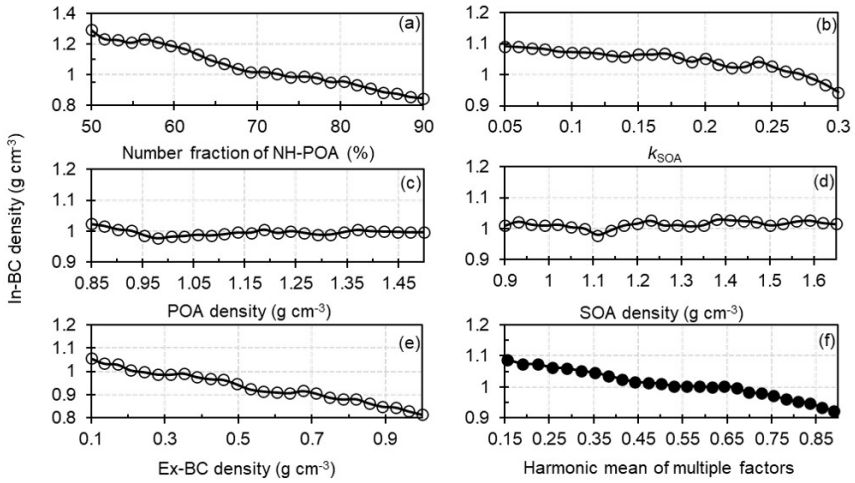

Figure 2. Sensitivity of the In-BC density to variations in the number fraction of nearly hydrophobic (NH) POA (a), the hygroscopic parameter of SOA (b), the POA density (c), the SOA density (d), the externally mixed BC density (e) and the harmonic mean of multiple factors (f).

The figures show that the In-BC density gradually decreases with the increment of the $NF_{NH\text{-}POA}$, implying the high fraction of bare POA particles correspond to the early aging stage of aerosol particles. With increase of κ_{SOA}, the In-BC density is generally reduced, but with small fluctuations (Fig.1a, Fig. 2b). This suggests a complex impact of assumptions of κ_{SOA} on the retrieved BC density. In addition, the In-BC density

删除了:

移动了(插入) [5]

删除了: higher

decreases slightly as $\rho_{Ex\text{-}BC}$ increases (Fig. 2e), suggesting applying a larger $\rho_{Ex\text{-}BC}$ would derive smaller values for In-BC density. The In-BC density is insensitive to the changes of the density of POA and SOA, showing an almost negligible effect on the retrieved results (Fig. 2c and d).

The uncertainty analysis shows that, by comparing the results based on the mean fractions of the $NF_{NH\text{-}POA}$ with a typical atmospheric observed range of 50-90 % for the $NF_{NH\text{-}POA}$ (Liu et al., 2021a), we show that the assumption on $NF_{NH\text{-}POA}$ can lead to relative deviations (uncertainty) of -17 %~+27 % for the retrieved BC density (Fig.3a).

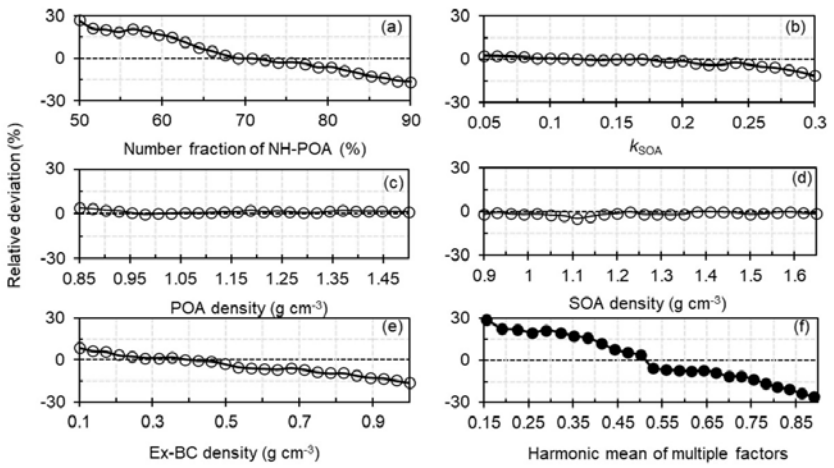

Figure 3. Relative deviations of the number fraction of nearly hydrophobic (NH) POA to the In-BC density (a), the hygroscopic parameter of OA to the In-BC density (b), the POA density to the In-BC density (c), the SOA density to the In-BC density (d), the externally mixed BC density to In-BC density (e) and the combined deviations based on multiple factors mentioned above (f).

In addition, unlike inorganics (eg., NH_4HSO_4, $(NH_4)_2SO_4$ and NH_4NO_3), which

删除了: very

上移了 [4]: **Figure 1.** Sensitivities of In-BC density to the variations in the number fraction of nearly hydrophobic (NH) POA and hygroscopic parameter of OA (k_{SOA}) (a), POA density (b), SOA density (c) and the externally mixed BC density (d).

上移了 [5]: **Figure 2.** Sensitivity of the In-BC density to variations in the number fraction of nearly hydrophobic (NH) POA (a), the hygroscopic parameter of SOA (b), the POA density (c), the SOA density (d), the externally mixed BC density (e) and the harmonic mean of multiple factors (f).

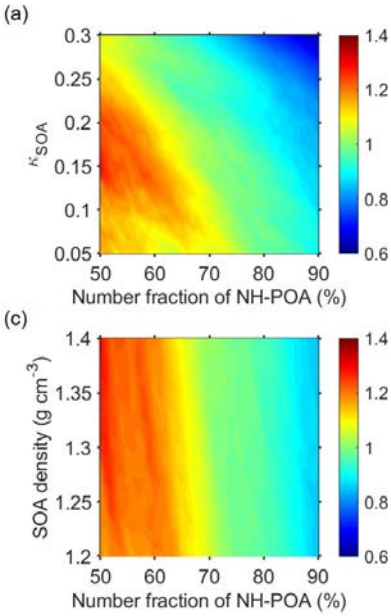

删除了:

删除了: ...

删除了: %–+

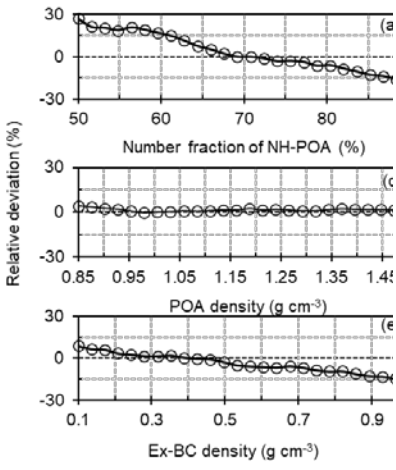

删除了:

the hygroscopicity has been already well-understood (Petters and Kreidenweis, 2007), the hygroscopicity of organic species varies largely due to the complexity in organic aerosol constituents. Therefore, the assumption of the values of κ_{SOA} will add the uncertainty in the calculation of BC density. Previous studies have suggested that the organics has a wide range of κ values ranging from 0.05 to 0.3 (Jimenez et al., 2009; Mei et al., 2013). Thus, the sensitivity test has also been done to examine the effect due to changes in κ_{SOA} on calculating the density of BC (Fig. 1a). The result shows that the assumption of κ_{SOA} value can cause an average relative deviation of -10 %~+3 % in calculating the density of In-BC (Fig. 3b).

However, the sensitivity test shows that the impact of both the ρ_{POA} and ρ_{SOA} variations on the BC density estimation is very small or even negligible (Fig. 1b, c). By varying the ρ_{POA} from 0.85 to 1.5 g cm^{-3} and the ρ_{SOA} from 0.9 to 1.65 g cm^{-3} according to the literatures (Noureddini et al., 1992; Alfarra et al., 2006; Reyes-Villegas et al., 2018; Cai et al., 2020; Kostenidou et al., 2007), the retrieval uncertainties in the BC density are both within ±5 % (Fig. 3c, d). For $\rho_{Ex\text{-}BC}$, it exhibits that the evolution of the $\rho_{Ex\text{-}BC}$ could lead to an average deviation of -16 %~+9 % in calculating In-BC density (Fig. 3e) when increasing the values of $\rho_{Ex\text{-}BC}$ from 0.1 to 1.0 g cm^{-3}, which represents a typical range in ambient atmosphere (Wu et al., 2019; Liu et al., 2020). A combined uncertainty (δ) caused by the multiple factors (δ_i), which is calculated by equation 12, is -26 %~+29 % as shown in Fig. 3f.

$$\delta = \sqrt{\sum_{i=1}^{n} {\delta_i}^2} \quad (12)$$

In addition, it should be noted that the mass concentration of BC obtained from

删除了: %~+

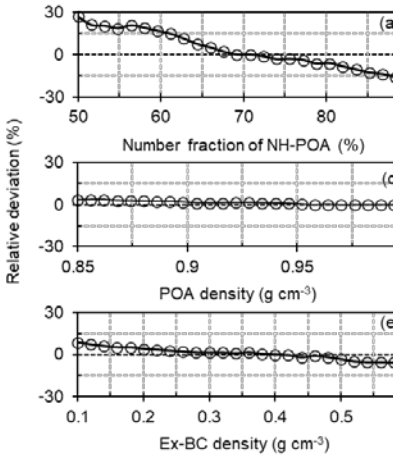

删除了:

Figure 3. Relative deviations of the number fraction of nearly hydrophobic (NH) POA to the In-BC density (a), the hygroscopic parameter of OA to the In-BC density (b), the POA density to the In-BC density (c), the SOA density to the In-BC density (d), the externally-mixed BC density to In-BC density (e) and the combined deviations based on multiple factors mentioned above (f).

删除了: 0

删除了: 1.2

删除了: 4

删除了: and ±1 % respectively

删除了: ±10

删除了: .6

删除了: 21 %~+

AE33 based on aerosol light absorption may lead some uncertainty. However, the comparison of the simultaneously measured data by SP2 with that by AE33 during the campaign shows that the temporal variations of BC mass concentrations measured by the two techniques are well consistent (Fig S5). Note that the BC mass measured by SP2 is occasionally low probably because of the low detection efficiency in small size (McMeeking et al., 2010; Schwarz et al., 2006). In addition, the SP2 is unable to quantify the BC mass beyond a certain limit because of the saturation of electronic devices recording signals (Pileci et al., 2021). We show that, compared the results that retrieved if applying the BC mass measured by SP2, the BC density retrieved based on AE33 can be 18% higher. Given that the measurement bias from SP2, this overestimation indicates an upper limit of the uncertainty.

3 Results and Discussion

3.1 Retrieved mixing state and density of BC: comparison and validation

Figure 4a shows retrieved time series of the mixing state of ambient BC during the campaign. Large temporal variations of the mass fraction of internally and externally mixed BC are presented during the observed period at the sites. The temporal changes should be related to the atmospheric aging process or diurnal variations of emissions (Liu et al., 2019a; Fan et al., 2020). Statistically, the average mass fraction of externally and internally mixed BC is 20±18 % and 80±20 % respectively, showing that most of the BC particles were aged and internally mixed with other components. Previous studies at urban sites have shown that the co-existence of the externally mixed BC in

the ambient atmosphere (Schwarz et al., 2008; Cheng et al., 2012; Chen et al., 2020) due to continuous combustion processes (e.g., vehicle exhaust and residential sector) (Wang et al., 2017; Liu et al., 2019a). Our results are basically comparable with those

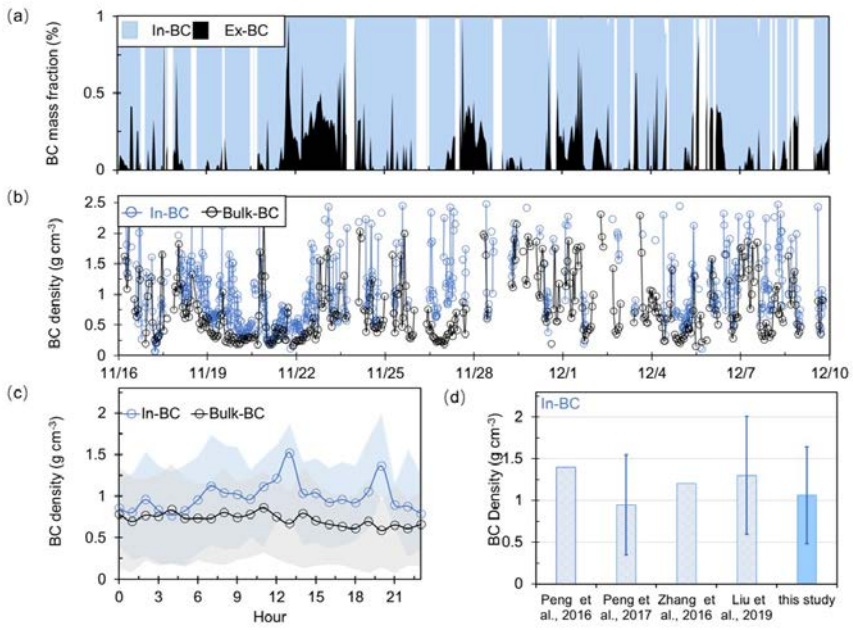

Figure 4. (a) Time series of the mass fraction of the retrieved internal- and external-mixed BC; (b) Time series of the retrieved density of the bulk and internal- mixed BC (In-BC); (c) Diurnal variation of the retrieved density of bulk and In-BC; (d) Comparison of the results of the derived In-BC density in this study with that reported in literatures.

previously reported results, which are directly measured or indirectly retrieved. For example, Chen et al., 2020 found that the mass fraction of internally mixed BC particles was nearly ~80–90 % in summer of Beijing based on VTDMA measurements. Liu et al. (2020), using a tandem system with an aerodynamic aerosol classifier and SP2, reported

删除了:

删除了: previously reported results

删除了: to be

that the mass fraction of internally BC-containing particles would increase with increasing size and reach ~70 % in Beijing. Overall, the mass fraction obtained in our study is comparable with those reported in urban Beijing. Previous studies also displayed that the significant diversity of the BC mixing state among emission conditions and coating process (Shiraiwa et al., 2008; Pan et al., 2017; Zhang et al., 2020b). Accordingly, the densities of the bulk and internally mixed BC present apparent fluctuations as shown in Fig. 4b, which is significantly affected by the variations of BC emission sources and its rapid aging process. The density of the In-BC during daytime was generally higher than that at night (Fig. 4c). The elevated BC density during daytime is likely due to that the strong photochemical processes promote the aging of BC particles, which resulted in a conversion from uncompacted structure to compact and regular spherical shapes of BC (Qiao et al., 2018; Liu et al., 2019b; Zhou et al., 2022). The lift in BC density around 20:00 LT might indicate that the BC particles would be rapidly coated with the secondary inorganic aerosol (SIA) particles and continuously aged in the polluted period due to the heterogeneous reactions of SIA in urban regions (Zhang et al., 2016; Peng et al., 2017). Actually, following the haze evolution, the fraction of nearly hydrophobic group reduced rapidly (Fig. S8). Consequently, the average density of In-BC increased obviously from the clean conditions to the polluted periods (Fig. S9). A slight decrease was observed in the bulk BC density during traffic hours. This is likely associated with the continues emissions (e.g., vehicle exhaust) that lead to uncoated or uncompacted BC particles in this period. The diurnal cycle in In-BC density is consistent with the coating thickness measured

删除了: S7

删除了: S8

by a tandem CPMA-SP2-DMA-SP2 (Liu et al., 2020), demonstrating that the new method can derive the density of ambient BC particles reasonably. Averagely, the bulk and internally mixed BC densities are with campaign averaged values of 0.7±0.5 and 1.1±0.6 g cm^{-3} respectively, which are much less than 1.8 g cm^{-3}, implying that the BC particles is not a void-free spheres in the urban atmosphere. The results of In-BC density are comparable with that observed at the other sites in North China Plain (NCP) as shown in Fig. 4d, illustrating that the BC effective density retrieved by this method is within the range of field measurements.

删除了:

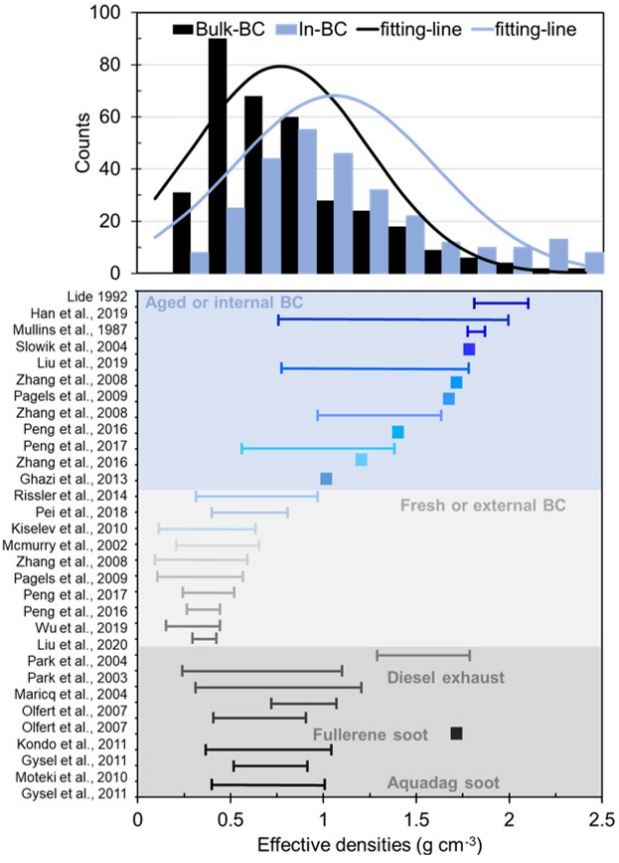

Figure 5. The probability distribution function (PDF) of the retrieved density of bulk

and In-BC and the measured density distribution spectrum of BC from different sources reported in literatures.

Based on both field measurements (e.g. Lide 1992; Zhang et al., 2016; Wu et al., 2019; Liu et al., 2019b) and laboratory studies (e.g. McMurry et al., 2002; Park et al., 2003, 2004; Olfert et al., 2007; Kiselev et al., 2010; Gysel et al., 2011, 2012), the BC density from diverse combustion sources or representing different aging degree has been obtained and ranges widely from 0.14 to 2.1 g cm^{-3}, as has been summarized and shown in Fig. 5. Mean probability distribution function (PDF) of the density of bulk and In-BC retrieved by this study is also presented in Fig. 5. It shows that the retrieved density of bulk BC exhibits a dominant mode with a peak value of 0.7 g cm^{-3}, which is situated between the typical density range of those externally mixed and internally mixed BC measured previously. For the In-BC, the PDF is with a peak value at 1.1 g cm^{-3}, but ranges widely from ~0.5 to 2.5 g cm^{-3}, which indicates various morphologies, different aging degree and compositions of ambient BC particles due to the complex impact of multiple local sources and aging processes during the observed period in urban Beijing. Overall, the retrieved values for In-BC density fall within the range of typical internal mixed BC reported in the literatures, verifying the reliability of our inversion results.

3.2 Sensitivity of predicted N_{CCN} to changes of BC density

A previous study showed that the use of an inaccurate density value of BC particles would result in large bias in estimating κ of ambient aerosol particles with the ZSR

mixing rule (Fan et al., 2020), as would further lead to uncertainties in prediction of N_{CCN} and relevant climate effects. Considering the large variation range of BC density during the campaign, which is closely associated with its morphology or degree of its aging, we further examine the sensitivity of critical supersaturation (S_c), critical diameter (D_{cut}) and predicted N_{CCN} to variations of BC density (Fig. 6). Here, we use the critical diameter and particle number size distribution to calculate N_{CCN}. The method to derive the critical diameter is based on Köhler theory and ZSR rule.

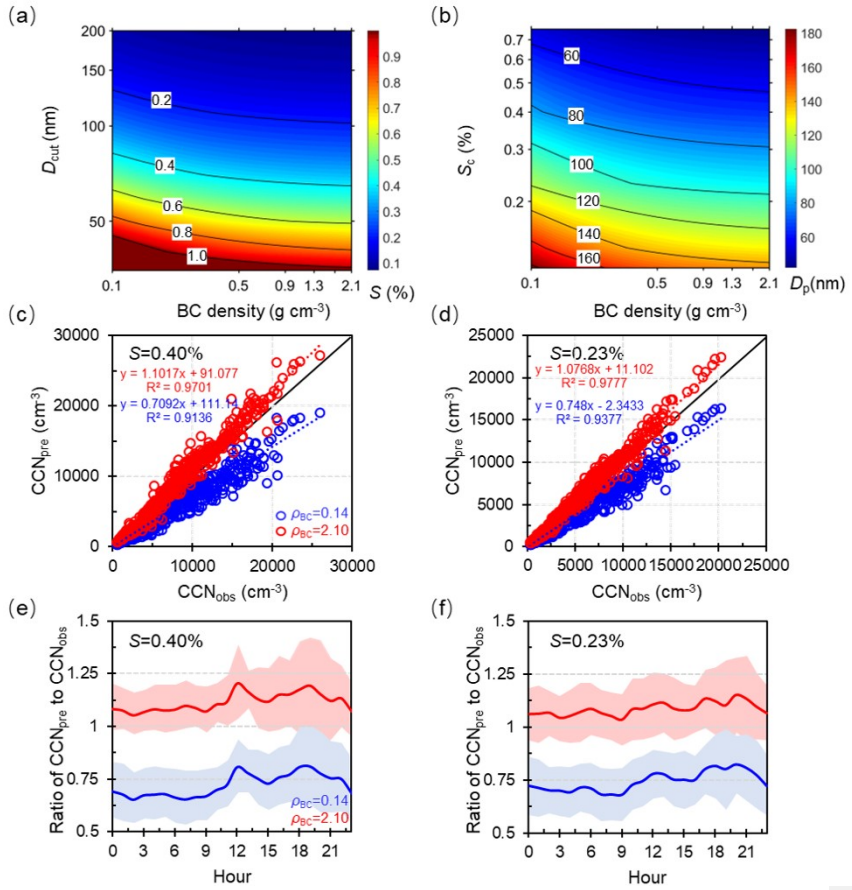

Figure 6. Sensitivity of critical supersaturation (S_c) (a) and diameter (D_{cut}) (b) to the

variations in BC density; Predicted N_{CCN} as a function of measured N_{CCN} by varying the density from 0.14 to 2.1 g cm^{-3} at S=0.40 % (c) and S=0.23 % (d), the black solid line is the 1:1 line; Diurnal variations in the ratio of predicted-to-measured N_{CCN} at S=0.40 % (e) and S=0.23 % (f).

The results show that, by varying the value of density from 0.14 to 2.1 g cm^{-3} that represents the lower and upper limit of BC density in the atmosphere, the D_{cut} reduces apparently at a given supersaturation (S) (Fig. 6a), or similarly, the S_c decreases rapidly for a given particle size (Fig. 6b). The results show that the changes of the D_{cut} and S_c are more sensitive when the BC density is below 1.0 g cm^{-3}. And the effects on the D_{cut} and S_c both gradually weakened with the increase of BC density. This shows that it is critical to apply more accurate BC density for the aerosol particles with low aging degree in predicting CCN and its climate effect. Accordingly, the ratios of predicted-to-measured N_{CCN} ranged from 0.72 to 1.11 by varying the BC density from 0.14 to 2.1 g cm^{-3} at the typical S of 0.23 % and 0.40 % (Fig. 6c, 6d), showing an estimation uncertainty of -28 % ~ 11 % in N_{CCN} prediction.

删除了: -

The diurnal variations in the ratio of predicted-to-measured N_{CCN} at S=0.40 % and 0.23 % are shown to examine the response of the BC density on N_{CCN} prediction at different time periods (Fig. 6e, 6f). By applying the lower limit of density value of 0.14 g cm^{-3}, the prediction is much worse compared to the use of the density of 2.1 g cm^{-3} at nighttime (00:00-06:00 LT), when the latter is much closer to the real density of ambient BC (Fig. 4c). The prediction is improved substantially by applying the value of 0.14 g cm^{-3} during evening rush hours (18:00-20:00 LT), during which the ambient BC

particles is disturbed by the traffic emissions (Fig. 4c). And now, the prediction becomes worse by applying the value of 2.1 g cm^{-3}, and an obvious overestimation by up to ~40 % is shown. The results further illustrate that it is critical to account for the real-time mixing state and density of BC particles in N_{CCN} prediction, particularly in those regions with heavy traffic and residential coal emissions.

It should be noted that the assumption of the surface tension of water would overestimate the critical diameter and underpredict CCN number concentration. While the surface tension depression might be more obvious for the small size particles (<60 nm), as the fraction of organics are higher at small particles size (Meng et al., 2014; Cai et al., 2018). Here, in this study, we calculated the critical diameters at supersaturations of 0.40 % and 0.23 %, typical values in cloud, corresponding to larger sizes (> 70 nm and 90 nm) of aerosols. Therefore, the uncertainties from the application of the surface tension of pure water should be negligible (< 10 %). Here, three schemes were assumed to evaluate the effect of BC density and mixing state on prediction of CCN number concentrations. The detailed calculation methods are presented in the supporting information (SI: Methods) or referenced from Ren et al. (2018).

删除了: .,

删除了: .

3.3 Using the real-time variations of BC density and mixing state to predict N_{CCN}

Figure 7 exhibits the comparisons between predicted and measured N_{CCN} at S of 0.23 % and 0.40 % by accounting for the retrieved real-time variations of BC density and mixing state. It shows that the N_{CCN} can be well predicted with a slope of 1.01 and 1.02 at S of 0.23 % and 0.40 % respectively (Fig. 7a, 7b), only presenting a slight

deviation. The slight deviation is primarily due to the fixed value of the density for the externally mixed BC caused by the retrieved method, especially during noontime and evening rush periods (Fig. 7c and 7d).

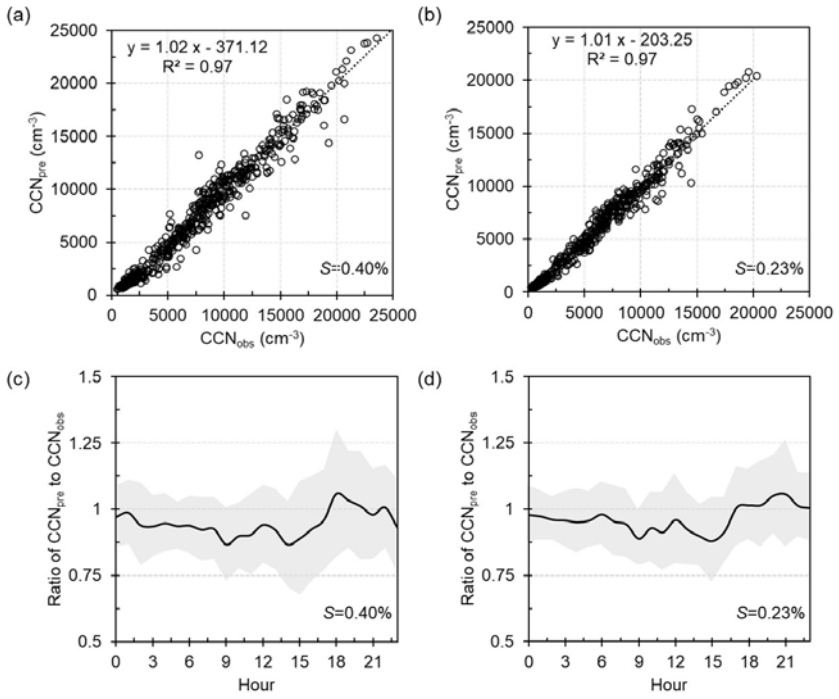

Figure 7. Prediction CCN number concentration using the mixing state and In-BC density derived from HTDMAs at S=0.40 % (a) and S=0.23 % (b). Diurnal variations in the ratio of predicted-to-measured N_{CCN} at S=0.40 % (c) and S=0.23 % (d).

The diurnal variations in the ratio of predicted-to-measured N_{CCN} shows the N_{CCN} can be underestimated by up to 15 % at S=0.40 % during those periods. While, a slightly overrated during the evening traffic hours and nighttime may be due to the underestimation of the number fraction of Ex-BC. Overall, the dependence of the CCN prediction on S is due to the size dependence of κ and mixing state (Zhang et al., 2017;

Liu et al., 2020; Xu et al., 2021). The better closure at S=0.23 % is because that the bulk κ of particles is closer to that the critical diameter corresponding to S=0.23 %, with D_p of 100-150 nm. Similarly, the effect on CCN prediction induced by the bulk mixing state would be more critical for smaller particles, corresponding to the critical diameter at high S.

Overall, when considering the effective density of BC relevant to its mixing state, the CCN closure achieves. Previous studies have shown that the fresh emitted BC particles may convert from fractal-like aggregates to a compact structure and its density would increase with the aging process (Pagels et al., 2009; Rissler et al., 2014; Peng et al., 2016; Liu et al., 2019b; Zhang et al., 2020a, 2022), but the actual density of In-BC may be lower than 1.8 g cm^{-3} in the ambient atmosphere according to this study. Therefore, the currently applied value represents a density of the void-free structure of BC particles may cause an overestimation in CCN prediction.

4 Conclusions

The mixing state and effective density of BC changed through heterogenous chemistry process and thus would cause uncertainty in evaluating its CCN activity. In this study, we develop a new method to retrieve the mixing state and effective density of ambient BC using field measurements and the Köhler theory. The uncertainty of the new retrieval method was evaluated within ±30 %, which is primarily caused by assuming the value of κ_{SOA} and the fraction of primary organic aerosols in non-hygroscopic mode. The retrieved results show that most of the BC particles were aged

删除了: to

删除了: hygroscopic or

and internally mixed with other components, with mean mass fraction of 80±20 %. Averagely, the retrieved densities of the bulk and internally mixed BC are 0.7±0.5 and 1.1±0.6 g cm^{-3} respectively, but ranges widely from ~0.1 to 2.5 g cm^{-3}, indicating various morphologies, different aging degree and compositions of ambient BC particles due to the complex impact of multiple local sources and aging processes during the observed period. The retrieved results are basically comparable with the previous observations in North China Plain.

Further examination shows the N_{CCN} prediction is with uncertainties of -28 % ~11 % at the typical S of 0.23 % and 0.40 % by varying the BC density from 0.14 to 2.1 g cm^{-3} that represents the lower and upper limit of ambient BC particles. Moreover, the prediction is found more sensitive to the variability of BC density when it is <1.0 g cm^{-3}, suggesting a great significance to account for the effect of BC density for the aerosol particles with low aging degree when evaluating the climate effect. The CCN closure achieves when introducing the retrieved real-time BC density relevant to its mixing state. This work provides a unique way of utilizing field observations to infer ambient BC density and highlights the current assumption of a void-free structure of BC particles in models would cause large uncertainties in CCN prediction and in the relevant climate effect evaluation.

The method used to derive the ambient BC density has limitations. Since the assumptions on the values of κ_{SOA}, ρ_{POA}, ρ_{SOA} and $\rho_{Ex\text{-}BC}$ as well as the fraction of primary organic aerosols in non-hygroscopic or hygroscopic mode would add uncertainty in the inferred values of ambient internally mixed BC density. It is thus

删除了: internal-

删除了: –

necessary to examine observational data to verify this methodology in further studies. However, the method and results of this study could provide the way for a more comprehensive understanding of the variability in BC density in Beijing. Additionally, it has the potential to reveal the uncertainties of usage of void-free structure of BC density in accessing the climate effects.

Data availability.

All data needed to evaluate the conclusions in the paper are present in the paper and/or the Supplement. All data used in the study are also available from the corresponding author upon request (zhangfang2021@hit.edu.cn).

Author contributions.

FZ and JR conceived the conceptual development of the manuscript. JR directed and performed of the experiments with JL, LC, and FZ. JR conducted the data analysis and wrote the draft of the manuscript. All authors edited and commented on the various sections of the manuscript.

Acknowledgments.

This work was funded by the National Natural Science Foundation of China (NSFC) research project (41975174, 41675141). We thank all participants in the field campaigns for their tireless work and cooperation. We also thank Dr. Yele Sun and his group for

providing the data of nonrefractory submicron aerosol chemical composition.

Competing interests.

The contact author has declared that neither they nor their co-authors have any competing interests.

References

Alfarra, M. R., Paulsen, D., Gysel, M., Garforth, A. A., Dommen, J., Prévôt, A. S. H., Worsnop, D. R., Baltensperger, U., and Coe, H.: A mass spectrometric study of secondary organic aerosols formed from the photooxidation of anthropogenic and biogenic precursors in a reaction chamber, Atmos. Chem. Phys., 6, 5279– 5293, https://doi:10.5194/acp-6-5279-2006, 2006.

Bond, T. C., Doherty, S. J., Fahey, D., Forster, P., Berntsen, T., DeAngelo, B., Flanner, M., Ghan, S., Kärcher, B., and Koch, D.: Bounding the role of black carbon in the climate system: A scientific assessment, J. Geophys. Res.-Atmos., 118(11), 5380–5552, https://doi.org/10.1002/jgrd.50171, 2013

Clarke, A.D., Shinozuka, Y., Kapustin, V.N., Howell, S., Huebert, B., Doherty, S., Anderson, T., Covert, D., Anderson, J., Hua, X., Moore II, K.G., McNaughton, C., Carmichael, G., Weber, R.: Size distributions and mixtures of dust and black carbon aerosol in Asian outflow: physiochemistry and optical properties, J. Geophys. Res.-Atmos., 109, D15S09, https://doi.org/10.1029/2003JD004378, 2004.

Cheng, Y. F., Su, H., Rose, D., Gunthe, S. S., Berghof, M., Wehner, B., Achtert, P., Nowak, A., Takegawa, N., Kondo, Y., Shiraiwa, M., Gong, Y. G., Shao, M., Hu, M., Zhu, T., Zhang, Y. H., Carmichael, G. R., Wiedensohler, A., Andreae, M. O., and Pöschl, U.: Size-resolved measurement of the mixing state of soot in the megacity Beijing, China: diurnal cycle, aging and parameterization, Atmos. Chem. Phys., 12, 4477–4491, https://doi.org/10.5194/acp-12-4477-2012, 2012.

Cheng, Y. F., Eichler, H., Wiedensohler, A., Heintzenberg, J., Zhang, Y. H., Hu, M., Herrmann, H., Zeng, L. M., Liu, S., Gnauk, T., Brüggemann, E., and He, L. Y.: Mixing state of elemental carbon and non-light-absorbing aerosol components derived from in situ particle optical properties at Xinken in Pearl River Delta of China, J. Geophys. Res., 111, D20204, doi:10.1029/2005JD006929, 2006.

Chen, L., F. Zhang, P. Yan, X. Wang, L. Sun, Y. Li, X. Zhang, Y. Sun, and Z. Li.: The large proportion of black carbon (BC)-containing aerosols in the urban atmosphere, Environ. Pollut., 263, 114507, https://doi.org/10.1016/j.envpol.2020.114507, 2020.

Chang, R. Y.-W., Slowik, J. G., Shantz, N. C., Vlasenko, A., Liggio, J., Sjostedt, S. J.,

Leaitch, W. R., and Abbatt, J. P. D.: The hygroscopicity parameter (*k*) of ambient organic aerosol at a field site subject to biogenic and anthropogenic influences: relationship to degree of aerosol oxidation, Atmos. Chem. Phys., 10, 5047–5064, https://doi:10.5194/acp-10-5047-2010, 2010.

Cai, M., Tan, H., Chan, C. K., Qin, Y., Xu, H., Li, F., Schurman, M. I., Liu, L., and Zhao, J.: The size-resolved cloud condensation nuclei (CCN) activity and its prediction based on aerosol hygroscopicity and composition in the Pearl Delta River (PRD) region during wintertime 2014, Atmos. Chem. Phys., 18, 16419–16437, https://doi.org/10.5194/acp-18-16419-2018, 2018.

Cai, J., Chu, B., Yao, L., Yan, C., Heikkinen, L. M., Zheng, F., Li, C., Fan, X., Zhang, S., Yang, D., Wang, Y., Kokkonen, T. V., Chan, T., Zhou, Y., Dada, L., Liu, Y., He, H., Paasonen, P., Kujansuu, J. T., Petäjä, T., Mohr, C., Kangasluoma, J., Bianchi, F., Sun, Y., Croteau, P. L., Worsnop, D. R., Kerminen, V.-M., Du, W., Kulmala, M., and Daellenbach, K. R.: Size-segregated particle number and mass concentrations from different emission sources in urban Beijing, Atmos. Chem. Phys., 20, 12721–12740, https://doi.org/10.5194/acp-20-12721-2020, 2020.

Dinar, E., Mentel, T. F., and Rudich, Y.: The density of humic acids and humic like substances (HULIS) from fresh and aged wood burning and pollution aerosol particles, Atmos. Chem. Phys., 6, 5213–5224, doi:10.5194/acp-6-5213-2006, 2006.

Dameto de España, C., Wonaschütz, A., Steiner, G., Rosati, B., Demattio, A., Schuh, H., and Hitzenberger, R.: Long-term quantitative field study of New Particle Formation (NPF) events as a source of Cloud Condensation Nuclei (CCN) in the urban background of Vienna, Atmos. Environ., 164, 289–298, https://doi.org/10.1016/j.atmosenv.2017.06.001, 2017.

Flanner, M. G., Zender, C. S., Randerson, J. T., and Rasch, P. J.: Present-day climate forcing and response from black carbon in snow, J. Geophys. Res.-Atmos., 112, D11202, https://doi.org/10.1029/2006JD008003, 2007.

Fan, X., Liu, J., Zhang, F., Chen, L., Conllins, D., Xu, W., Jin, X., Ren, J., Wang, Y.,Wu, H., Li, S., Sun, Y., Li, Z.: Contrasting size-resolved hygroscopicity of fine particles derived by HTDMA and HR-ToF-AMS measurements between summer and winter in Beijing: the impacts of aerosol aging and local emissions, Atmos. Chem. Phys. 20, 915-929, https://doi.org/10.5194/acp-20-915-2020, 2020.

Geller, M., Biswas, S., and Sioutas, C.: Determination of particle effective density in urban environments with a differential mobility analyzer and aerosol particle mass analyzer, Aerosol Sci. Technol., 40, 709–723, https://doi.org/10.1080/02786820600803925, 2006.

Gysel, M., McFiggans, G. B., and Coe, H.: Inversion of tandem differential mobility analyser (TDMA) measurements, J. Aerosol Sci., 40, 134–151, https://doi.org/10.1016/j.jaerosci.2008.07.013, 2009.

Gysel, M., Crosier, J., Topping, D. O., Whitehead, J. D., Bower, K. N., Cubison, M. J., Williams, P. I., Flynn, M. J., McFiggans, G. B., and Coe, H.: Closure study between chemical composition and hygroscopic growth of aerosol particles during TORCH2, Atmos. Chem. Phys., 7, 6131–6144, https://doi.org/10.5194/acp-7-6131-2007, 2007.

Gunthe, S. S., King, S. M., Rose, D., Chen, Q., Roldin, P., Farmer, D. K., Jimenez, J.

L., Artaxo, P., Andreae, M. O., Martin, S. T., and Pöschl, U.: Cloud condensation nuclei in pristine tropical rainforest air of Amazonia: size resolved measurements and modeling of atmospheric aerosol composition and CCN activity, Atmos. Chem. Phys., 9, 7551–7575, https://doi.org/10.5194/acp-9-7551-2009, 2009.

Gysel, M., Laborde, M., Olfert, J. S., Subramanian, R., & Gröhn, A. J.: Effective density of aquadag and fullerene soot black carbon reference materials used for SP2 calibration, Atmos. Meas. Tech., 4(12), 4937–4955, https://doi.org/10.5194/amt-4-2851-2011, 2011.

Gysel, M., Laborde, M., Mensah, A. A., Corbin, J. C., Keller, A., Kim, J., et al.: Technical note: The single particle soot photometer fails to reliably detect PALAS soot nanoparticles, Atmos. Meas. Tech., 5(12), 3099–3107, https://doi.org/10.5194/amt-5-3099-2012, 2012.

Jimenez, J. L., Canagaratna, M. R., Donahue, N. M., Prevot, A. S. H., Zhang, Q., Kroll, J. H., DeCarlo, P. F., Allan, J. D., Coe, H., Ng, N. L., Aiken, A. C., Docherty, K. S., Ulbrich, I. M., Grieshop, A. P., Robinson, A. L., Duplissy, J., Smith, J. D., Wilson, K. R., Lanz, V. A., Hueglin, C., Sun, Y. L., Tian, J., Laaksonen, A., Raatikainen, T., Rautiainen, J., Vaattovaara, P., Ehn, M., Kulmala, M., Tomlinson, J. M., Collins, D. R., Cubison, M. J., Dunlea, E. J., Huffman, J. A., Onasch, T. B., Alfarra, M. R., Williams, P. I., Bower, K., Kondo, Y., Schneider, J., Drewnick, F., Borrmann, S., Weimer, S., Demerjian, K., Salcedo, D., Cottrell, L., Griffin, R., Takami, A., Miyoshi, T., Hatakeyama, S., Shimono, A., Sun, J. Y., Zhang, Y. M., Dzepina, K., Kimmel, J. R., Sueper, D., Jayne, J. T., Herndon, S. C., Trimborn, A. M., Williams, L. R., Wood, E. C., Middlebrook, A. M., Kolb, C. E., Baltensperger, U., and Worsnop, D. R.: Evolution of Organic Aerosols in the Atmosphere, Science., 326, 1525–1529, https://doi.org/10.1126/science.1180353, 2009.

Kiselev, A., Wennrich, C., Stratmann, F., Wex, H., Henning, S., Mentel, T.F., Kiendler-Scharr, A., Schneider, J., Walter, S., Lieberwirth, I.: Morphological characterization of soot aerosol particles during LACIS Experiment in November (LExNo), J. Geophys. Res. -Atmos., 115, D11204. https://doi.org/10.1029/2009jd012635, 2010.

Khalizov, A. F., Zhang, R., Zhang, D., Xue, H., Pagels, J., and McMurry, P. H.: Formation of highly hygroscopic soot aerosols upon internal mixing with sulfuric acid vapor, J. Geophys. Res.-Atmos., 114, D05208, https://doi.org/10.1029/2008jd010595, 2009.

Kawana, K., Nakayama, T., and Mochida, M.: Hygroscopicity and CCN activity of atmospheric aerosol particles and their relation to organics: Characteristics of urban aerosols in Nagoya, Japan, J. Geophys. Res.-Atmos., 121, 4100–4121, https://doi.org/10.1002/2015JD023213, 2016.

Kostenidou, E., Pathak, R. K., & Pandis, S. N.: An Algorithm for the Calculation of Secondary Organic Aerosol Density Combining AMS and SMPS Data, Aerosol Science and Technology, 41:11, 1002-1010, https://doi: 10.1080/02786820701666270, 2007.

Li, M., Zhang, Q., Kurokawa, J.-I., Woo, J.-H., He, K., Lu, Z., Ohara, T., Song, Y., Streets, D. G., Carmichael, G. R., Cheng, Y., Hong, C., Huo, H., Jiang, X., Kang, S., Liu, F., Su, H., and Zheng, B.: MIX: a mosaic Asian anthropogenic emission

769 inventory under the international collaboration framework of the MICS-Asia and
770 HTAP, Atmos. Chem. Phys., 17, 935–963, https://doi.org/10.5194/acp-17-935-2017,
771 2017.
772 Liu, D., Joshi, R., Wang, J., Yu, C., Allan, J. D., Coe, H., Flynn, M. J., Xie, C., Lee, J.,
773 Squires, F., Kotthaus, S., Grimmond, S., Ge, X., Sun, Y., and Fu, P.: Contrasting
774 physical properties of black carbon in urban Beijing between winter and summer,
775 Atmos. Chem. Phys., 19, 6749–6769, https://doi.org/10.5194/acp-19-6749-2019,
776 2019a.
777 Liu, D., Allan, J., Whitehead, J., Young, D., Flynn, M., Coe, H., McFiggans, G.,
778 Fleming, Z. L., and Bandy, B.: Ambient black carbon particle hygroscopic properties
779 controlled by mixing state and composition, Atmos. Chem. Phys., *13*, 2015–2029,
780 https://doi.org/10.5194/acp-13-2015-2013, 2013.
781 Liu, H., Pan, X.L., Wu, Y., Wang, D.W., Tian, Y., Liu, X.Y., et al.: Effective densities of
782 soot particles and their relationships with the mixing state at an urban site in the
783 Beijing megacity in the winter of 2018, Atmos. Chem. Phys. 19, 14791–14804,
784 https://doi.org/10.5194/acp-19-14791-2019, 2019b.
785 Lide, D. R. (ed.). CRC Handbook of Chemistry and Physics. CRC Press: Ann Arbor,
786 MI. (1992).
787 Lance, S., Medina, J., Smith, J., and Nenes, A.: Mapping the operation of the DMT
788 continuous flow CCN counter, Aerosol Sci. Tech., 40, 242–254,
789 https://doi.org/10.1080/02786820500543290, 2006.
790 Liu, H., Pan, X., Liu, D., Liu, X., Chen, X., Tian, Y., Sun, Y., Fu, P., and Wang, Z.:
791 Mixing characteristics of refractory black carbon aerosols at an urban site in Beijing,
792 Atmos. Chem. Phys., 20, 5771–5785, https://doi.org/10.5194/acp-20-5771-2020,
793 2020.
794 Liu, L, Zhang, J, Zhang, Y, Wang, Y, Xu, L, Yuan, Q, et al.: Persistent residential
795 burning-related primary organic particles during wintertime hazes in North China:
796 insights into their aging and optical changes, Atmos. Chem. Phys. *21*, 2251–2265,
797 https://doi.org/10.5194/acp-21-2251-2021, 2021a.
798 Liu, J., Zhang, F., Xu, W., Sun, Y., Chen, L., Li, S.: Hygroscopicity of organic aerosols
799 linked to formation mechanisms, Geophysical Research Letters, 48, e2020GL091683,
800 https://doi.org/10.1029/2020gl091683, 2021b.
801 McMurry, H. Peter, Wang Xin, Park Kihong & Ehara Kensei.: The Relationship
802 between Mass and Mobility for Atmospheric Particles: A New Technique for
803 Measuring Particle Density, Aerosol Sci. Technol., 36:2, 227-238,
804 https://doi.10.1080/027868202753504083, 2002.
805 Massoli, P., Onasch, T.B., Cappa, C.D., Nuamaan, I., Hakala, J., Hayden, K., Li, S.M.,
806 Sueper, D.T., Bates, T.S., Quinn, P.K., Jayne, J.T., Worsnop, D.R.: Characterization
807 of black carbon-containing particles from soot particle aerosol mass spectrometer
808 measurements on the R/V Atlantis during CalNex 2010, J. Geophys. Res.- Atmos.,
809 120, 2575-2593, https://doi.org/10.1002/2014JD022834, 2015.
810 Mei, F., Setyan, A., Zhang, Q., and Wang, J.: CCN activity of organic aerosols observed
811 downwind of urban emissions during CARES, Atmos. Chem. Phys., 13, 12155–
812 12169, https://doi.org/10.5194/acp-13-12155-2013, 2013.

Meng, J. W., Yeung, M. C., Li, Y. J., Lee, B. Y. L., and Chan, C. K.: Size-resolved cloud condensation nuclei (CCN) activity and closure analysis at the HKUST Supersite in Hong Kong, Atmos. Chem. Phys., 14, 10267–10282, https://doi.org/10.5194/acp-14-10267-2014, 2014.

McMeeking, G.R., Hamburger, T., Liu, D., Flynn, M., Morgan, W.T., Northway, M., Highwood, E.J., Krejci, R., Allan, J.D., Minikin, A., Coe, H.: Black carbon measurements in the boundary layer over western and northern Europe. Atmos. Chem. Phys. 10, 9393-9414, https://doi.org/10.5194/acp-10-9393-2010, 2010.

Noureddini, H., Teoh, B. C., Davis Clements, L.: Densities of vegetable oils and fatty acids, J. Am. Oil Chem. Soc., 69 (12), 1184−1188, 1992.

Olfert, J. S., Symonds, J. P. R., and Collings, N.: The effective density and fractal dimension of particles emitted from a light-duty diesel vehicle with a diesel oxidation catalyst, J. Aerosol Sci., 38, 69–82, https://doi.org/10.1016/j.jaerosci.2006.10.002, 2007.

Park, K., Kittelson, D. B., and McMurry, P. H.: Structural properties of diesel exhaust particles measured by transmission electron microscopy (TEM): Relationships to particle mass and mobility, Aerosol Sci. Technol., 38, 881–889, https://doi.org/10.1080/027868290505189, 2004.

Pagels, J., Khalizov, A.F., McMurry, P.H. and Zhang, R.Y.: Processing of soot by controlled sulphuric acid and water condensation-mass and mobility relationship, Aerosol Sci. Technol., 43, 629–640, https://doi.org/10.1080/02786820902810685, 2009.

Peng, J. F., Hu, M., Guo, S., Du, Z. F., Zheng, J., Shang, D. J., Zamora, M., Zeng, L. M., Shao, M., Wu, Y. S., Zheng, J., Wang, Y., Glen, C., Collins, D., Molina, M., and Zhang, R. Y.: Markedly enhanced absorption, and direct radiative forcing of black carbon under polluted urban environments, P. Natl. Acad. Sci. USA, 113(16), 4266–4271, https://doi.org/10.1073/pnas.1602310113, 2016.

Petters, M. D. and Kreidenweis, S. M.: A single parameter representation of hygroscopic growth and cloud condensation nucleus activity, Atmos. Chem. Phys., 7, 1961–1971, https://doi.org/10.5194/acp-7-1961-2007, 2007.

Paatero, P. and Tapper, U.: Positive matrix factorization: A nonnegative factormodel with optimal utilization of error estimates of data values, Environmetrics, 5, 111–126, 1994.

Peng, J. F., Hu, M., Guo, S., Du, Z. F., Zheng, J., M., Zeng, L. M., Shao, M., Wu, Y. S., Collins, D., Molina, M., and Zhang, R. Y.: Ageing and hygroscopicity variation of black carbon particles in Beijing measured by a quasi-atmospheric aerosol evolution study (QUALITY) chamber, Atmos. Chem. Phys., 17(17), 10333-10348, https://doi.org/10.5194/acp-17-10333-2017, 2017.

Pan, X.L., Kanaya, Y., Taketani, F., Miyakawa, T., Inomata, S., Komazaki, Y., et al.: Emission characteristics of refractory black carbon aerosols from fresh biomass burning: a perspective from laboratory experiments, Atmos. Chem. Phys., 17(21), 13001–13016, https://doi.org/10.5194/acp-17-13001-2017, 2017.

Park, K., Cao, F., Kittelson, D. B., & McMurry, P. H.: Relationship between particle

mass and mobility for diesel exhaust particles, Environ. Sci. Tehnol., 37, 577–583, https://doi.org/10.1021/es025960v, 2003.

Pileci, R. E., Modini, R. L., Bertò, M., Yuan, J., Corbin, J. C., Marinoni, A., Henzing, B., Moerman, M. M., Putaud, J. P., Spindler, G., Wehner, B., Müller, T., Tuch, T., Trentini, A., Zanatta, M., Baltensperger, U., and Gysel-Beer, M.: Comparison of co-located refractory black carbon (rBC) and elemental carbon (EC) mass concentration measurements during field campaigns at several European sites, Atmos. Meas. Tech., 14, 1379–1403, https://doi.org/10.5194/amt-14-1379-2021, 2021.

Qiao, K., Wu, Z., Pei, X., Liu, Q., Shang, D., Zheng, J., Du, Z., Zhu,W.,Wu, Y., Lou, S., Guo, S., Chan, C.K., Pathak, R.K., Hallquist, M., Hu, M.: Size-resolved effective density of submicron particles during summertime in the rural atmosphere of Beijing. China, J. Environ. Sci. (China) 73, 69–77. https://doi.org/10.1016/j.jes.2018.01.012, 2018.

Rissler, J., Nordin, E. Z., Eriksson, A. C., Nilsson, P. T., Frosch, M., Sporre, M. K., Wierzbicka, A., Svenningsson, B., Londahl, J., Messing, M. E., Sjogren, S., Hemmingsen, J. G., Loft, S., Pagels, J. H., and Swietlicki, E.: Effective Density and Mixing State of Aerosol Particles in a Near-Traffic Urban Environment, Environ. Sci. Technol., 48, 6300–6308, https://doi.org/10.1021/es5000353, 2014.

Riemer, N., Vogel, H., and Vogel, B.: Soot aging time scales in polluted regions during day and night, Atmos. Chem. Phys., 4, 1885–1893, https://doi.org/10.5194/acp-4-1885-2004, 2004.

Ramanathan, V. and Carmichael, G.: Global and regional climate changes due to black carbon, Nat. Geosci., 36, 221-227, https://doi.org/10.1038/ngeo156, 2008.

Ren, J., Zhang, F., Wang, Y., Collins, D., Fan, X., Jin, X., et al.: Using different assumptions of aerosol mixing state and chemical composition to predict CCN concentrations based on field measurements in urban Beijing, Atmos. Chem. Phys., 18, 6907–6921, https://doi.org/10.5194/acp-18-6907-2018, 2018.

Rader, D.J., McMurry, P.H.: Application of the tandem differential mobility analyzer to studies of droplet growth or evaporation, J. Geophys. Res.- Atmos., 17, 771-787, https://doi.org/10.1016/0021-8502(86)90031-5, 1986.

Reyes-Villegas, E., Bannan, T., Le Breton, M., Mehra, A., Priestley, M., Percival, C., Coe, H., and Allan, J. D.: Online Chemical Characterization of Food-Cooking Organic Aerosols: Implications for Source Apportionment, Environ. Sci. Technol., 52, 5308–5318, https://doi.org/10.1021/acs.est.7b06278, 2018.

Schwarz, J.P., Gao, R.S., Fahey, D.W., Thomson, D.S., Watts, L.A., Wilson, J.C., Reeves, J.M., Darbeheshti, M., Baumgardner, D.G., Kok, G.L., Chung, S.H., Schulz, M., Hendricks, J., Lauer, A., K€ archer, B., Slowik, J.G., Rosenlof, K.H., Thompson, T.L., Langford, A.O., Loewenstein, M., Aikin, K.C.: Single-particle measurements of midlatitude black carbon and light-scattering aerosols from the boundary layer to the lower stratosphere. J. Geophys. Res.: Atmosphere 111, D16207, https://doi.org/10.1029/2006JD007076, 2006.

Schwarz, J. P., Gao, R. S., Spackman, J. R., Watts, L. A., Thomson, D. S., Fahey, D. W., Ryerson, T. B., Peischl, J., Holloway, J. S., Trainer, M., Frost, G. J., Baynard, T., Lack, D. A., de Gouw, J. A., Warneke, C., and Del Negro, L. A.: Measurement

of the mixing state, mass, and optical size of individual black carbon particles in urban and biomass burning emissions, Geophys. Res. Lett., 35, L13810, https://doi.org/10.1029/2008GL033968, 2008.
Stokes, R. and Robinson, R.: Interactions in aqueous nonelectrolyte solutions, I. Solute-solvent equilibria, J. Phys. Chem.-US, 70, 2126–2131, 1966.
Sun, Y., Du, W., Fu, P., Wang, Q., Li, J., Ge, X., Zhang, Q., Zhu, C., Ren, L., Xu, W., Zhao, J., Han, T., Worsnop, D. R., and Wang, Z.: Primary, and secondary aerosols in Beijing in winter: sources, variations, and processes, Atmos. Chem. Phys., 16, 8309–8329, https://doi.org/10.5194/acp-16-8309-2016,2016.
Sun, Y. L., Wang, Z. F., Du, W., Zhang, Q., Wang, Q. Q., Fu, P. Q., Pan, X. L., Li, J., Jayne, J., and Worsnop, D. R.: Long term real-time measurements of aerosol particle composition in Beijing, China: seasonal variations, meteorological effects, and source analysis, Atmos. Chem. Phys., 15, 10149–10165, https://doi.org/10.5194/acp-15-10149-2015, 2015.
Shiraiwa, M., Kondo, Y., Moteki, N., Takegawa, N., Sahu, L., Takami, A., et al.: Radiative impact of mixing state of black carbon aerosol in Asian outflow, J. Geophys. Res.- Atmos., 113, D24210, https://doi.org/ 10.1029/2008JD010546, 2008.
Tan, H., Xu, H., Wan, Q., Li, F., Deng, X., Chan, P. W., Xia, D., and Yin, Y.: Design and application of an unattended multifunctional H-TDMA system, J. Atmos. Ocean. Tech., 30, 1136–1148, https://doi.org/10.1175/JTECH-D-12-00129.1, 2013.
Ulbrich, I. M., Canagaratna, M. R., Zhang, Q., Worsnop, D. R., and Jimenez, J. L.: Interpretation of organic components from Positive Matrix Factorization of aerosol mass spectrometric data, Atmos. Chem. Phys., 9, 2891–2918, https://doi.org/10.5194/acp-9- 2891-2009, 2009.
Wang, Y., Wan, Q., Meng, W., Liao, F., Tan, H., and Zhang, R.: Long-term impacts of aerosols on precipitation and lightning over the Pearl River Delta megacity area in China, Atmos. Chem. Phys., 11, 12421–12436, https://doi.org/10.5194/acp-11-12421-2011, 2011.
Wang, Y. Y., Liu, F. S., He, C. L., Bi, L., Cheng, T. H., Wang, Z. L., Zhang, H., Zhang, X. Y., Shi, Z. B., and Li, W. J.: Fractal dimensions and mixing structures of soot particles during atmospheric processing, Environ. Sci. Tech. Lett., 4, 487–493, https://doi.org/10.1021/acs.estlett.7b00418, 2017.
Wu, Y. F., Xia, Y. J., Huang, R. J., Deng, Z. Z., Tian, P., Xia, X. G., et al.: A study of the morphology and effective density of externally mixed black carbon aerosols in ambient air using a size-resolved single-particle soot photometer (SP2), Atmos. Meas. Tech., 12, 4347–4359, https://doi.org/10.5194/amt-12-4347-2019, 2019.
Wu, Y., Wang, X., Tao, J., Huang, R., Tian, P., Cao, J., Zhang, L., Ho, K.-F., Han, Z., and Zhang, R.: Size distribution and source of black carbon aerosol in urban Beijing during winter haze episodes, Atmos. Chem. Phys., 17, 7965–7975, https://doi.org/10.5194/acp-17-7965-2017, 2017.
Wu, Z. J., Zheng, J., Shang, D. J., Du, Z. F., Wu, Y. S., Zeng, L. M., Wiedensohler, A., and Hu, M.: Particle hygroscopicity and its link to chemical composition in the urban atmosphere of Beijing, China, during summertime, Atmos. Chem. Phys., 16, 1123–1138, https://doi.org/10.5194/acp-16-1123-2016, 2016.

Xue, H., Khalizov, A. F., Wang, L., Zheng, J., and Zhang, R.: Effects of dicarboxylic acid coating on the optical properties of soot, Phys. Chem. Chem. Phys., 11, 7869–7875, https://doi.org/10.1039/b904129j, 2009.

Xu, W., Sun, Y., Wang, Q., Zhao, J., Wang, J., Ge, X., et al.: Changes in aerosol chemistry from 2014 to 2016 in winter in beijing: Insights from high-resolution aerosol mass spectrometry, J. Geophys. Res.-Atmos., 124, 1132–1147. https://doi.org/10.1029/2018jd029245, 2019.

Xu, W., Fossum, K. N., Ovadnevaite, J., Lin, C., Huang, R.-J., O'Dowd, C., and Ceburnis, D.: The impact of aerosol size-dependent hygroscopicity and mixing state on the cloud condensation nuclei potential over the north-east Atlantic, Atmos. Chem. Phys., 21, 8655–8675, https://doi.org/10.5194/acp-21-8655-2021, 2021.

Yuan, T., Li, Z., Zhang, R., and Fan, J.: Increase of cloud droplet size with aerosol optical depth: An observation and modeling study, J. Geophys. Res.-Atmos., 113, D04201, https://doi.org/10.1029/2007JD008632, 2008.

Yu, C., Liu, D., Broda, K., Joshi, R., Olfert, J., Sun, Y., Fu, P., Coe, H., Allan, J.D.: Characterising mass-resolved mixing state of black carbon in Beijing using a morphology-independent measurement method, Atmos. Chem. Phys., 20, 3645–3661. https://doi.org/10.5194/acp-20-3645-2020, 2020.

Zhang, R. Y., Khalizov, A. F., Pagels, J., Zhang, D., Xue, H. X., and McMurry, P. H.: Variability in morphology, hygroscopicity, and optical properties of soot aerosols during atmospheric processing, P. Natl. Acad. Sci. USA, 105, 10291–10296, https://doi.org/10.1073/pnas.0804860105, 2008.

Zhang, Y., Zhang, Q., Cheng, Y., Su, H., Kecorius, S., Wang, Z., Wu, Z., Hu, M., Zhu, T., Wiedensohler, A., and He, K.: Measuring the morphology and density of internally mixed black carbon with SP2 and VTDMA: new insight into the absorption enhancement of black carbon in the atmosphere, Atmos. Meas. Tech., 9, 1833–1843, https://doi.org/10.5194/amt-9-1833-2016, 2016.

Zdanovskii, A.: New methods for calculating solubilities of electrolytes in multicomponent systems, Zh. Fiz. Khim.C, 22, 1475– 1485, 1948.

Zhang, F., Wang, Y., Peng, J., Ren, J., Collins, D., Zhang, R., et al.: Uncertainty in predicting CCN activity of aged and primary aerosols, J. Geophys. Res.-Atmos., 122(21), 11723–11736, https://doi.org/10.1002/2017jd027058, 2017.

Zhang, F., Ren, J., Fan, T., Chen, L., Xu, W., Sun, Y., et al.: Significantly enhanced aerosol CCN activity and number, J. Geophys. Res.-Atmos., 124, 14102–14113, https://doi.org/10.1029/2019jd031457, 2019.

Zhang, F., Wang, Y., Peng, J., Chen, L., Sun, Y., Duan, L., Ge, X., Li, Y., Zhao, J., Liu, C., Zhang, X., Zhang, G., Pan, Y., Wang, Y., Zhang, A. L., Ji, Y., Wang, G., Hu, M., Molina, M. J., Zhang, R.: An unexpected catalyst dominates formation and radiative forcing of regional haze, P. Natl. Acad. Sci. USA, 117(8), 3960-3966, https://doi.org/10.1073/pnas.1919343117, 2020a.

Zhang, Y., Zhang, Q., Yao, Z., Li, H.: Particle Size and Mixing State of Freshly Emitted Black Carbon from Different Combustion Sources in China, Environ. Sci. Technol., 54(13): p. 7766-7774, https://doi.org/10.1021/acs.est.9b07373, 2020b.

Zhang, F., Peng, J., Chen, L., Collins, D., Li, Y., Jiang, S., Liu, J., Zhang, R.: The effect of Black carbon aging from NO2 oxidation of SO2 on its morphology, optical and

hygroscopic properties, Environ. Res., 212, 113238, https://doi.org/10.1016/j.envres.2022.113238, 2022.

Zhang, R., Wang, G., Guo, S., Zamora, M. L., Ying, Q., Lin, Y.: Formation of urban fine particulate matter, Chemical Reviews, 115(10), 3803–3855, https://doi.org/10.1021/acs.chemrev.5b00067, 2015.

Zhou, Y., Ma, N., Wang, Q., Wang, Z., Chen, C., Tao, J., Hong, J., Peng, L., He, Y., Xie, L., Zhu, S., Zhang, Y., Li, G., Xu, W., et al.: Bimodal distribution of size-resolved particle effective density: results from a short campaign in a rural environ ment over the North China Plain, Atmos. Chem. Phys., 22, 2029–2047. https://doi.org/10.5194/acp-22-2029-2022, 2022.

Zhao, G., Tan, T., Hu, S., Du, Z., Shang, D., Wu, Z., Guo, S., Zheng, J., Zhu, W., Li, M., Zeng, L., and Hu, M.: Mixing state of black carbon at different atmospheres in north and southwest China, Atmos. Chem. Phys., 22, 10861–10873, https://doi.org/10.5194/acp-22-10861-2022, 2022.